TALLINN UNIVERSITY OF TECHNOLOGY

School of Science

Department of Marine Systems

CHARACTERIZATION OF SUBMESOSCALE AND MESOSCALE FEATURES IN THE BALTIC SEA USING HIGH RESOLUTION SATELLITE SEA SURFACE TEMPERATURE FIELDS AND MODEL SIMULATIONS

Master's thesis

Eneli Toodu

Supervisors: Germo Väli, PhD

Rivo Uiboupin, PhD

Tallinn

2017

Declaration

Hereby I declare that this master's thesis, my original investigation and achievement, submitted for the master's degree at Tallinn University of Technology has not been submitted for any academic degree. All content and ideas drawn directly or indirectly from external sources are indicated as such.

Eneli Toodu
(Signature and date)

Supervisor: Germo Väli
Work meets the requirements for master's thesis.
(Signature and date)

The defence chief:
Accepted for defence of a thesis .....
Name, signature, date

TALLINNA TEHNIKAÜLIKOOL

Loodusteaduskond

Meresüsteemide instituut

SUB- JA MESOMASTAAPSETE NÄHTUSTE KIRJELDAMINE LÄÄNEMERES KASUTADES KÕRGLAHUTUSEGA SATELLIIDIPILTIDE JA HÜDRODÜNAAMIKA MUDELI PINNAVEE TEMPERATUURI ANDMEID

Magistritöö

Eneli Toodu

Juhendajad: Germo Väli, PhD

Rivo Uiboupin, PhD

Tallinn

2017

TABLE OF CONTENTS

Abstract

Mesoscale and submesoscale structures in the Baltic Sea surface layer were investigated using temperature data from different satellite products – Landsat and MODerate Resolution Imaging Spectroradiometer (MODIS), and from a 3D General Estuarine Transport Model (GETM) simulation. GETM and Landsat data were quantitatively compared with MODIS data to characterize the differences. Systematic error in Landsat due to constant bias between observed temperature values was detected and an empirical algorithm was constructed to derive high resolution sea surface temperature (SST) fields from brightness temperature in Landsat measurements. Relatively high correlation (0.9) between MODIS SST, Landsat SST and GETM SST was detected along with mean absolute differences less than 1 ^{o}C. Similar spatial variability and co-located mesoscale structures were revealed by qualitative comparison between the datasets. Significantly strong SST gradient magnitudes with large variability were seen at Landsat images, while MODIS and GETM gradient magnitudes were relatively low and did not contain small eddies. The spectral slope in 4−10 km range was the steepest for the simulated SST (mean slope −4.89) and the shallowest in the MODIS observations (mean slope −2.52). A comparison of spectral slopes for different areas in the Baltic Sea from Landsat SST in high frequency range (0.15−2 km) revealed slope in the Gulf of Finland about −2.52, in the Gulf of Riga −2.04 and in the Baltic Proper −1.71.

Keywords: sub- and mesoscale features, sea surface temperature, remote sensing and hydrodynamic simulations, statistical analysis, Baltic Sea

LÜHIKOKKUVÕTE

Käesolevas töös uuriti sub- ja mesomastaapseid struktuure Läänemere pinnakihis erinevate satelliidisensorite – Landsat ja *MODerate Resolution Imaging Spectroradiometer* (MODIS) ja 3D hüdrodünaamika mudeli (GETM) andmete põhjal. Leidmaks GETM'i ja Landsat'i erinevused MODIS'e andmetest, võrreldi andmeid kvantitatiivselt. Landsat'i andmetest leiti süstemaatiline viga, mis väljendus konstantses temperatuuride erinevuses. Landsat'i heledustemperatuuri andmete korrigeerimiseks leiti empiiriline algoritm, et saada kõrglahutuslikud pinnavee temperatuuri väljad. Leiti väga kõrge korrelatsioon (0.9) MODIS'e ja Landsat'i ning GETM'i ja MODIS'e pinnavee temperatuuri andmete vahel, samuti jäi keskmine absoluutne erinevus alla 1 ^{o}C. Kvalitatiivse analüüsi tulemusel leiti, et andmete vahel on ka ruumiline sarnasus, kus mesomastaapsed kujutised asusid samades kohtades. Landsat'i piltidelt oli näha, et pinnavee temperatuuri absoluutsed gradiendid olid väga tugevad ja absoluutse gradiendi väärtused varieerusid suurtes piirides ning võis eristada väikese mastaabiga keeriseid. MODIS'e ja GETM'i absoluutsete gradientide väärtused olid väikesed ning väärtuste jaotuse piltidelt ei olnud väikse mastaabiga keerised eristatavad. Spektrikalle vahemikus 4−10 km (mesomastaap) oli kõige järsem GETM'i pinnavee temperatuuri väljades (keskmiselt –4.89) ja kõige laugem MODIS'e mõõtmisandmete korral (keskmiselt –2.52). Erinevate basseinide võrdluses leiti, et Landsat'i spektrikalle submesomastaapses vahemikus (0.15−2 km) oli Soome lahes keskmiselt −2.52, Liivi lahes −2.04 ja Läänemere avaosas −1.71.

Võtmesõnad: meso- ja submesomastaapsed nähtused, pinnavee temperatuur, kaugseire ja hüdrodünaamika mudeli simulatsioonide andmed, statistiline analüüs, Läänemeri

1 INTRODUCTION

The Baltic Sea is a semi-enclosed intra-continental shallow sea located in northeast Europe. The Baltic Sea is one of the largest brackish water areas in the world with the mean salinity about 7 ‰. The mean depth of the Baltic Sea is 54 meters and the deepest point is the Landsort Deep (459 m) in the Western Gotland Basin, southeast of Stockholm. The surface area is 392 978 m^2 (Leppäranta and Myrberg 2009). Dynamics of the Baltic Sea are driven by momentum and heat fluxes from the atmosphere, river runoff, bottom topography, seasonal ice, coastline and boundary flows through the Danish Straits (Mälkki and Tamsalu 1985). The Baltic Sea has significant fresh-water surplus by river runoff and limited water exchange with the North Sea via the narrow and shallow Danish Sounds (Matthäus and Franck 1992). As a result, the Baltic Sea water column is strongly stratified restricting vertical mixing. The summer seasonal thermocline is located at a depth of 15−30 m, however, the seasonal thermocline starts to develop in the southern Baltic Sea at the beginning of May and in the Bay of Bothnia a month later. In autumn, thermocline starts deepening due to cooling and in the north it starts in late August whereas in the south a month later (Leppäranta and Myrberg 2009).

The mesoscale flow field in the ocean (10−100 km) has been studied extensively for its dynamics and its contribution to the lateral transport of heat, momentum and tracers via eddies and currents. Processes at length scales less than a kilometre (0.1−100 m) contribute to mixing and energy dissipation (Thomas et al. 2008). Processes which lie intermediate to meso- and small-scale are called submesoscale and those are less studied. Based on submesoscale dynamics, they could be defined as those where the bulk Rossby number, $Ro_b = U/fL$ and the bulk Richardson

number, $Ri_b = N^2H^2/U^2$, are both of the order of unity. Here U is the characteristic speed, H is the characteristic vertical length scale and L is the characteristic horizontal length scale of the velocity field, f is the Coriolis parameter, $N=\sqrt{-\frac{g}{\rho}\frac{d\rho}{dz}}$ is buoyancy frequency (Brunt-Väisälä frequency), where ρ is the potential density, which depends on temperature and salinity and g is the acceleration due to gravity (Thomas et al. 2008). According to the authors submesoscale is not described appropriately by the traditional quasi-geostrophic theory that applies to mesoscales.

Sub- and mesoscale structures are closely related due to the turbulent nature of oceanic flows, where energy is transferred between smaller and larger scales (Ferrari and Wunsch 2009). Phenomena with a horizontal scale approximately of the baroclinic Rossby radius of deformation are generally referred as mesoscale. Mesoscale variations of currents exist in almost every part of the world ocean (e.g. Robinson 1983). Nearly all seawater property fields such as temperature, salinity, density and concentrations of constituents show mesoscale patterns. Various mesoscale structures have been discovered in the Baltic Sea such as intra-pycnocline anticyclonic lenses, subsurface cyclonic eddies – negative lenses and "ordinary" upper layer cyclonic and anticyclonic eddies (e.g. Reißmann 2005, 2006). In the Baltic Sea the baroclinic Rossby radius of deformation (R_1) is in the range from 1 to 10 km (Fennel et al. 1991), whereas in the Gulf of Finland R_1 is usually 2–4 km (Alenius et al. 2003; Soomere et al. 2008). The larger R_1 values were determined in the deeper water areas (Alenius et al. 2003).

Mesoscale and submesoscale processes have been studied in the Baltic Sea using satellite sea surface temperature (SST) imagery from NOAA/AVHRR, MODerate Resolution Imaging Spectroradiometer (MODIS) on board of Terra and Aqua or Landsat satellites (e.g. Kahru et al. 1995; Uiboupin and Laanemets 2009; Lehmann et al. 2012; Karimova et al. 2012). Also, *in situ* measurements (e.g. Vahtera et al 2005; Lips and Lips 2014) and numerical modelling (e.g. Andrejev and Sokolov

2010; Laanemets et al. 2011; Lehmann et al. 2012; Väli et al 2016) have been used for characterizing mesoscale and submesoscale features in the Baltic Sea.

Väli et al. (2016) used Princeton Ocean Model with different horizontal resolutions in the Gulf of Finland to investigate submesoscale dynamics during series of coastal upwelling events in summer 2006. They found that simulation with the grid size of 0.125 nautical miles (~230 m) revealed different forms of submesoscale structures in the gulf's surface layer such as high Rossby number (Ro>1) threads, cyclonic vortices with core of 4−6 km diameter and spiral cyclonic eddies of 10–15 km diameter. They also analysed power spectral density of temperature and velocity fluctuations in the surface layer which showed some increase of spectral levels and shallowing of spectral slope towards –2 in the log-log space on the submesoscale (shorter) wavelengths. Lips et al (2016) have used *in situ* temperature data with spatial resolution of 160 m for spectral analysis. Data were collected by Ferrybox in the Gulf of Finland surface layer. They found that that the wavenumber spectra of temperature variance in the surface layer had slopes varying mostly between –3.7 and –1.8 in horizontal scales from 0.5 to 10 km.

A number of studies have been carried out in the World ocean and in the Baltic Sea where remote sensing data has been used for identifying and characterising submesoscale dynamics in the surface layer (Karimova et al. 2012; Bouffard et al. 2012; Gurova et al. 2012; Alpers et al. 2013; Ohlmann et al. 2017). Karimova et al. (2016) have used manual identifying for sub- and mesoscale eddies from satellite RGB optical images and SAR (synthetic aperture radar) data with pixel spacing of 75 m. They visually inspected 6878 mesoscale and submesoscale eddies in the Baltic Sea from Envisat ASAR images acquired in 2009–2011.

Liu et al. (2015) investigated submesoscale processes in the western South China Sea using MEdium Resolution Imaging Spectrometer (MERIS) data with resolution of 300 m and MODIS data with resolution of 1000 m. However, submesoscale flows in the ocean are defined to be with horizontal scales ranging from 0.1 to 10 km

(Buckingham et al. 2015), which allows to assess submesoscale flows in the oceans with lower spatial resolution. In the sea areas where baroclinic Rossby radius of deformation is small, like Baltic Sea, it is important to use the highest resolution data to investigate submesoscale processes. Ohlmann et al. (2017) used drifter observations to study submesoscale flow kinematics near the west end of Catalina Island, located about 30 km off the Southern California coast and they identified submesoscale features observed by drifters and remotely sensed SST with 1 km resolution.

According to Charney (1971) the spectral slope in case of quasi-geostrophic theory is –3 in the log-log space in mesoscale range. High-resolution simulations showed spectral slope of –2 in the submesoscale range (Capet et al. 2008; Brannigan et al. 2015; Väli et al. 2016).

The objectives of this study are: (1) to retrieve high resolution SST fields from Landsat thermal infrared (TIR) spectral band; (2) to validate/compare the Landsat SST with standard MODIS SST product; (3) to characterize submesoscale structures from the high resolution satellite imagery and model fields by applying gradient analysis (Quentel et al. 2010; Karimova and Gade 2016) and power spectral density analysis (Brannigan et al. 2015; Lips et al. 2016; Väli et al. 2016;).

2 MATERIALS AND METHODS

2.1 Satellite data processing

In this study, sea surface temperature (SST) data from different satellites was used. The 4-year (2012−2015) data measured either by MODIS onboard of Terra and Aqua satellites was compared with data from Landsat 7 and Landsat 8 satellites. In total, 25 images from each dataset at the 2012−2015 period were used.

Terra and Aqua overpass the Baltic Sea daily. MODIS Level 2 products provide SST calculated from long (11−12 μm) and the short (3−4 μm) wavelength bands with approximately 1000 m resolution (OceanColor Web, 2015). It is confirmed from previous studies that the MODIS SST measurements have the accuracy of up to ± 0.5 ^{o}C (Brown and Minnett 1999; Reinart and Reinhold 2008; Uiboupin and Laanemets 2015). In present study, SST images from the ice-free period were analysed and used as a reference for SST. Cloud mask and quality flags included in MODIS Level 2 SST product were implemented to mask the invalid pixels (Feldman 2016).

The brightness temperature fields from Landsat 7 were calculated by using band 6 with the wavelength 10.40−12.50 μm and 30 m horizontal resolution. Landsat 8 thermal infrared (TIRS) band 10 which has a 10.60−11.19 μm wavelength and 30 m resolution was also used to retrieve high resolution brightness temperature fields. The top of atmosphere (TOA) reflectance was converted to the brightness temperature according to USGS (2016). To relate the band 6 brightness temperature

to SST an empirical relation was derived for each month using collocated MODIS SST data. In addition to SST calculation, cloud masking algorithm by Oreopoulos et al. (2011) was implemented. Further supervised thresholding was implemented to eliminate cloud contamination on Landsat SST fields. In case of Landsat 8 TIRS band the quality assessment band was also used for cloud masking.

2.2 Numerical model

The General Estuarine Transport Model (GETM, Burchard et al. 2004) has been applied to simulate the seasonal SST patterns and dynamics in the central Baltic Sea. GETM is a primitive equation 3-dimensional, free surface, hydrostatic model with a vertically adaptive coordinate scheme (Hofmeister et al. 2010; Gräwe et al. 2015) embedded. Vertical mixing is parameterized by two equation k-ε turbulence model coupled to an algebraic second-moment closure (Canuto et al. 2001; Burchard and Bolding 2001). The implementation of the turbulence model is done via General Ocean Turbulence Model (GOTM, Umlauf and Burchard 2005).

The horizontal step of the model grid was 0.5 nautical miles (approximately 926 m) in the whole modelling domain (Figure 1); there were 60 adaptive levels in the vertical direction. The digital topography of the Baltic Sea was taken from Baltic Sea Bathymetry Database (Baltic Sea Hydrographic Commission 2013) and corrected for the Gulf of Finland from Andrejev et al. (2010, 2011).

Atmospheric forcing (wind stress and surface heat flux components) were calculated from wind, solar radiation, air temperature, total cloudiness and relative humidity data taken from HIRLAM (High Resolution Limited Area Model) version of the Estonian Weather Service with the spatial resolution of 11 km and forecast interval of 1 h ahead of 54 h, recalculated after every 6 h (Männik and Merilain 2007). Wind velocity components at the 10 m level along with other HIRLAM meteorological parameters were interpolated to the model grids.

Model simulations were performed from 01 April to 30 September for different years in period 2011−2015 covering the seasonal cycle of SST and other processes in the Baltic Sea including formation of the thermocline. The model domain has a closed boundary for the simulation period in the Danish straits (by an artificial shore) during all simulated years (2012−2015). The freshwater input from 27 largest Baltic Sea rivers with interannual variability was taken into account.

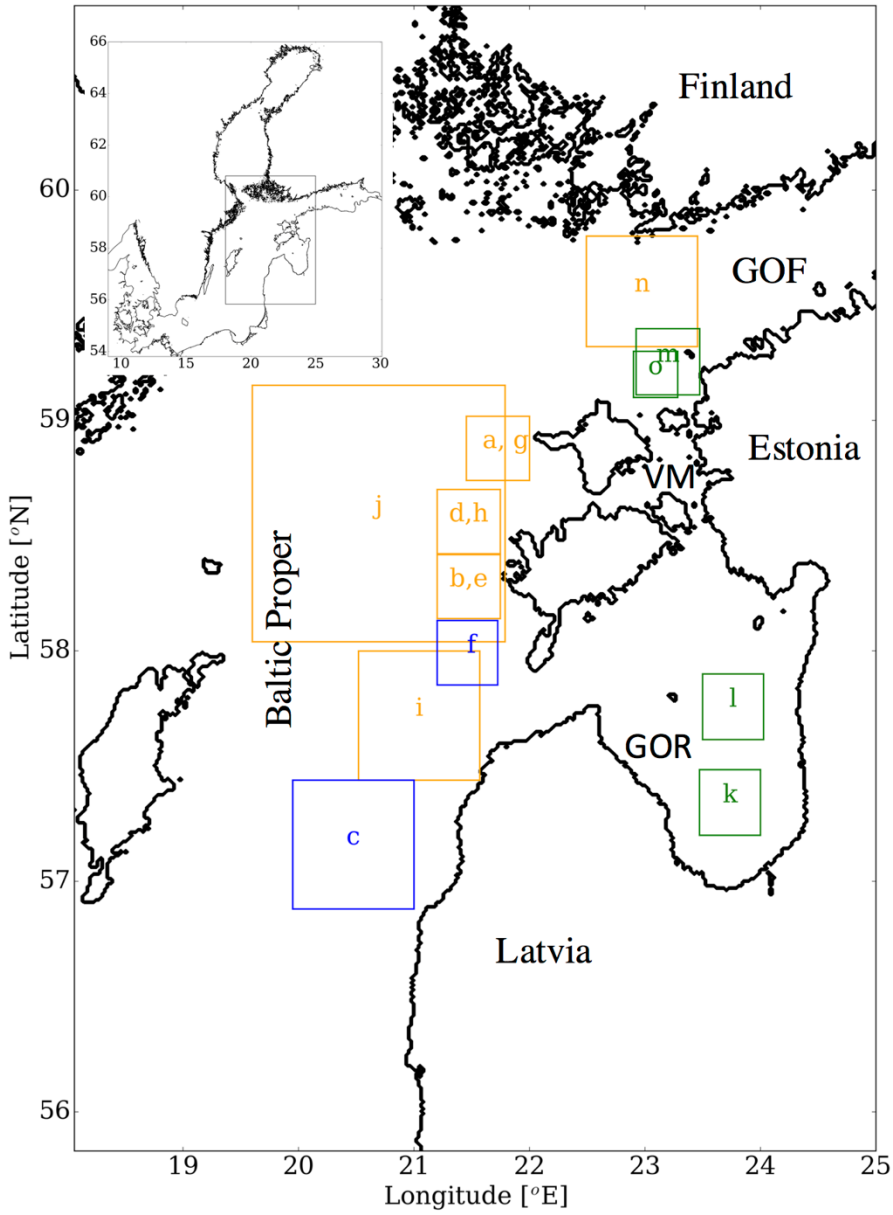

Figure 1. Map of Baltic Sea (upper left corner) with zoom to the area of interest. Coloured subsets are locations where power spectral analysis was made and different locations are distinguished by letters from a to o. Yellow boxes indicate subsets with Landsat, GETM and MODIS data available, blue boxes subsets with Landsat and GETM data available and green subsets with only Landsat data available. Note that subset e) had only GETM and Landsat data. VM indicates to Väinameri, GOF to Gulf of Finland and GOR to Gulf of Riga.

2.3 Statistical parameters

The brightness temperature fields from Landsat and GETM simulated SST fields were compared with MODIS Level 2 SST product, which was considered as the reference. MODIS SST product has been thoroughly validated against *in situ* measurements in numerous studies (e.g. Brown and Minnett 1999; Reinart and Reinhold 2008; Uiboupin and Laanemets 2015). The following statistical parameters were calculated for validation of Landsat and GETM data: mean value and variance of each temperature field, mean difference (MD), mean absolute difference (MAD), root mean square difference (RMSD) and correlation coefficient (R).

In this study, data for constructing the correction algorithm for Landsat were chosen by the following criteria: (a) the correlation between MODIS and Landsat should be more than 0.35; (b) mean absolute difference (MAD) should be less than 2 ^{o}C; (c) time difference between adjacent satellite overpass less than 36 hours; (d) cloud cover less than 40%; (e) there should be at least 100 data points from the same location.

In addition to qualitative comparison, with these estimations, the reliability of GETM and Landsat SST was assessed. After the statistical comparison of MODIS SST and Landsat brightness temperature fields, a bias correction was applied to Landsat brightness temperature fields to retrieve high resolution SST fields.

For the retrieval of high resolution SST fields from Landsat imagery and for bias correction of these fields, the Landsat and MODIS data was interpolated to a common regular MODIS grid with horizontal resolution of 1000 meters. A linear

regression was applied to daily means of Landsat brightness temperatures and MODIS SST data.

Taylor diagram was used to visualize the discrepancy between Landsat and GETM from MODIS. Taylor diagram provide a concise statistical summary of how well data patterns match each other, using correlation, RMSD and the ratio of variances (Taylor 2001). According to the author the diagram works on the principle that correlation coefficient R, the centred pattern RMS error E' and the standard deviation σ_f and σ_r between datasets have a geometric relationship.

Meso- and submesoscale dynamical quantities in the upper oceanic layer are known to display certain spectral slope of power spectral density (PSD) in wavenumber space. However, to characterise the spatial distribution of the examined quantity (SST), the power law must be determined between the wavenumber and energy in a logarithmic space for the scale between 0.15−10 km in the Baltic Sea. Thus, in order to estimate power law slopes, a two-dimensional (2D) Fast Fourier Transform (FFT) was applied to the image subsets. Prior to spectrum calculations, the Hanning window with the α value of 0.5 was applied to the input data. No other smoothing was used. The equivalent one-dimensional (1D) spectrum was obtained by integrating spectral coefficients in concentric rings in 2D wavenumber space. Spectral density was calculated from Landsat, MODIS and GETM data, whereas different subsets were chosen from the areas where there was no impact from clouds or land and from high frequency noise.

Spectral slope for MODIS and GETM SST was calculated within a range from 4−10 km (low frequency range), which was range from wavelengths four times the grid spacing to reduce domain-scale and grid-scale effects to 10 km (corresponding to wavenumbers from range from $10^{-3.6}$ to 10^{-4}). For Landsat low frequency range is 2−10 km (corresponding to wavenumbers from range from $10^{-3.3}$ to 10^{-4}) and high

frequency range is 0.15−2 km (corresponding to wavenumbers from range from $10^{-2.2}$ to $10^{-3.3}$).

In addition, gradient magnitudes of SST from MODIS, GETM and Landsat data were analysed in the areas with strong fronts. Gradients were calculated in ^{o}C per km. Other than that gradient distributions were analysed with histograms and gradients intensities from different datasets were compared.

3 RESULTS AND DISCUSSION

3.1 Statistical comparison

Landsat and GETM SST fields were quantitatively compared with MODIS data to ensure their concurrence and to construct an empirical algorithm for deriving high resolution SST fields from Landsat brightness temperature field.

The bias between MODIS and Landsat and GETM was calculated and is shown in Figure 2. The overall bias distribution patterns differed significantly. In general, the simulated SST values were slightly underestimated, the mean bias was –0.028 ^{o}C and standard deviation 0.95 ^{o}C (absolute differences exceeded up to 4 ^{o}C), while the high resolution brightness temperature fields were strongly overestimated with the mean bias 2.17 ^{o}C and standard deviation 1.01 ^{o}C (absolute differences exceeded 5 ^{o}C). On the other hand, the relatively high Landsat bias suggested that the brightness temperature can be corrected by a simple empirical algorithm to derive SST values.

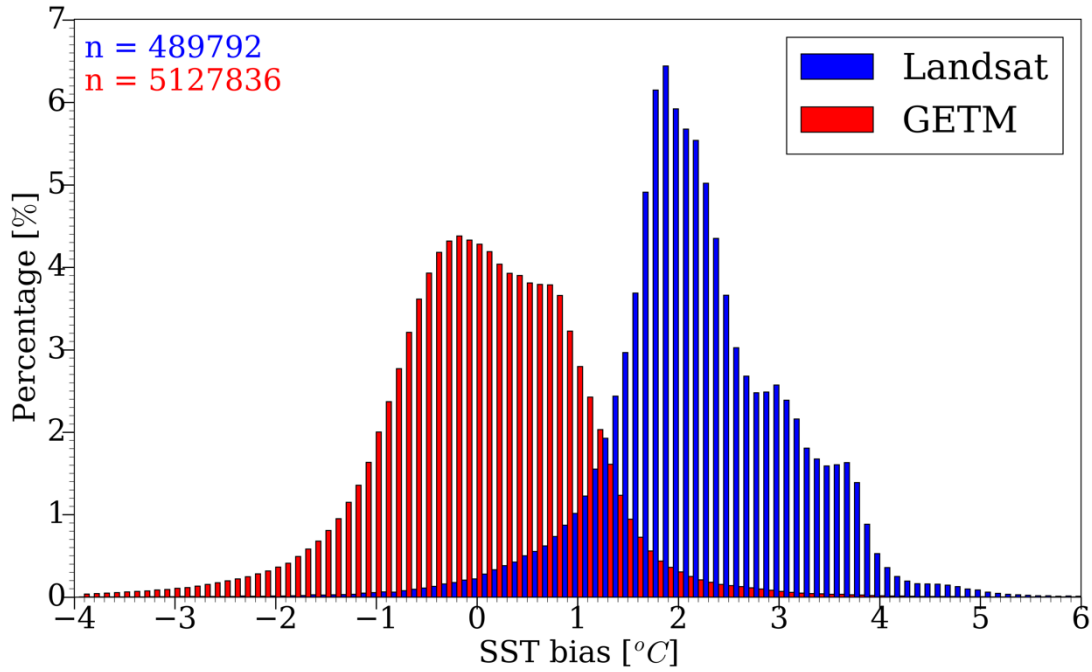

Figure 2. Frequency of temperature bias between MODIS and Landsat (MODIS – Landsat, blue bars) and MODIS and GETM (MODIS – GETM, red bars). Corresponding number of used data points is written on figure.

Monthly algorithms for converting Landsat brightness temperature to SST were derived using linear regression analysis over data from years 2012–2015 (Table 1). The largest amount of data was for the August with observations for 6 different dates and the lowest number of data was for the June, when there was only one day with usable data. In total the number of available data points varied from 20312 to 169608 for different months (Table 1).

Monthly correlations between Landsat and MODIS SST were relatively high, but varied significantly. The highest value of 0.93 was for the September and lowest value of 0.62 for July. Mean absolute difference varied from 0.30 (April) to 0.78 ^{o}C (August) and root mean square difference from 0.41 (April) to 0.95 ^{o}C (August). The standard deviation of Landsat was underestimated. The largest difference was in June, when there was only data from one day available.

Table 1. Comparison between the MODIS and Landsat SST fields. MD – mean difference (°C), MAD – mean absolute difference (°C) and RMSD – root mean square difference (°C), R – correlation between Landsat and MODIS. DIM – days in month used for analysis. σ is the standard deviation (°C), while subscript M marks to MODIS and L marks Landsat.

Month	MD	MAD	RMSD	R	σ_M	σ_L	n	DIM	Linear equation
April	0.11	0.30	0.41	0.87	0.79	0.79	84154	3	0.89x + 2.17
May	–0.12	0.66	0.93	0.92	2.25	2.08	45008	5	0.96x + 1.55
June	0.08	0.35	0.54	0.67	0.70	0.33	20312	1	0.51x + 6.17
July	–0.15	0.76	0.92	0.63	1.15	1.12	102016	5	0.83x + 5.12
August	0.07	0.78	0.95	0.77	1.41	1.02	169608	6	0.86x + 4.27
September	0.08	0.58	0.78	0.93	2.24	1.96	88942	5	0.83x + 5.17

Simulated (GETM) and measured (MODIS) SST was reasonably well correlated – the correlation was within a range from 0.68 to 0.94 (Table 2). The largest values were in May, when the Baltic was rapidly warming due to seasonal solar heating and in August when the heat content in the upper mixed layer reached the maxima while the lowest correlation was in July (0.68). The mean absolute difference between the GETM and MODIS SST was less than 1 °C, while the simulated SST were underestimated for the most of the year – from April to July and overestimated for the August and September. Similarly, with the MD and MAD, the RMSD was close to 1 °C varying from 0.82 to 1.09 °C and reached maximum value in July. The simulated SST standard deviation varied from 1.13 to 2.29 °C and measured SST from 1.27 to 2.44 °C with largest differences (0.28 °C) between each other in July and smallest (0.05 °C) in August. MODIS and GETM had corresponding data points from 144093 to 983516 in different months (Table 2).

Table 2. Same as in Table 1 for GETM and MODIS comparison. No correction algorithm was used for GETM data.

Month	MD	MAD	RMSD	R	σ_M	σ_G	n	DIM
April	0.56	0.78	0.92	0.85	1.34	1.13	429974	3
May	0.52	0.81	0.97	0.94	2.44	2.29	597653	5
June	0.19	0.68	0.91	0.85	1.57	1.65	144093	1
July	0.16	0.86	1.09	0.68	1.27	1.55	503440	5
August	–0.12	0.59	0.82	0.91	1.96	1.91	983516	6
September	–0.93	1.00	1.23	0.86	1.72	1.64	561050	5

Data was also analysed and visualized as daily averaged collocated values (see Figure 3). The application of SST correction algorithm to Landsat data reduced slightly the offset to value 0.21 ^{o}C, which was smaller than offset between the simulated and measured SST (value –0.49 ^{o}C). In addition, the Landsat SST was slightly overestimated, while the simulated SST was underestimated. The correlation between MODIS and Landsat and MODIS and GETM data was extremely large (0.99).

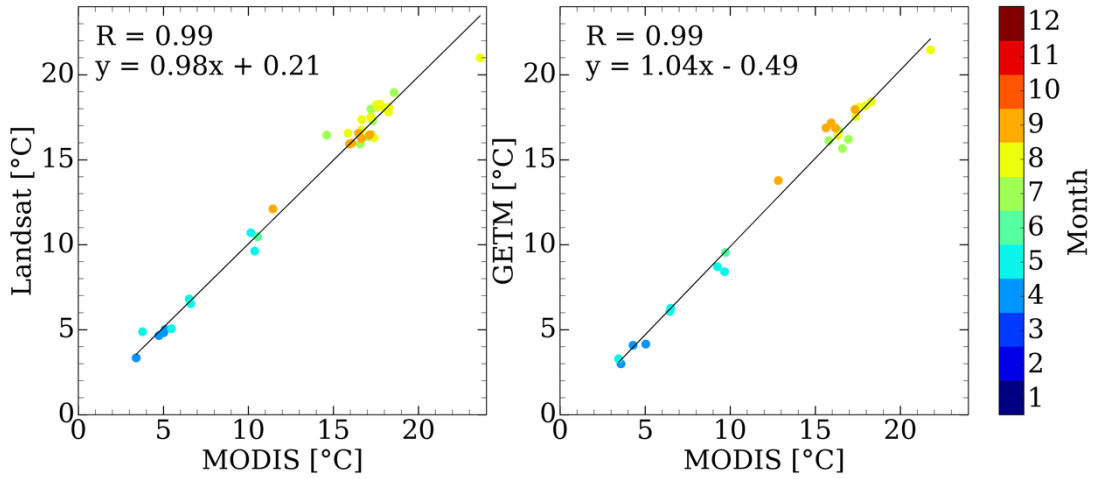

Figure 3. Daily averaged scatter plots of SST data from MODIS versus Landsat (left) and MODIS versus GETM (right). Data points are coloured based on month value, which the value represents.

Statistical differences between Landsat, GETM and MODIS SST data are summarized on Taylor diagrams (Figure 4). In general, simulated SST statistical parameters were relatively close to observed SST statistical parameters during all the months (see different panels in Figure 4), while high resolution SST fields were more scattered. The highest coincidence of the high resolution SST fields was during May (Figure 4b), when Landsat and MODIS data STD ratio for different days was within range 0.8–1.25 and maximum RMSD was less than 1.2 of observed STD. The overall difference in variability was 0.9 (the variability in Landsat SST fields in May was lower than observed variability), while the RMSD was 0.4 of observed STD. The lowest precision in Landsat measurements was in June (Figure 4c), when only one day of high resolution SST fields was available. The overall day to day variability indicated that Landsat SST fields underestimated the spatial variability by more than 50% (in June) or overestimated it by more than 40% (April - Figure 4a). Although, there were some days with larger discrepancy between high resolution SST fields and MODIS data, the overall quality of the high resolution data was reasonable. The highest RMSD between day-to-day values in Landsat and MODIS data was 1.2 of observed STD and lowest less than 0.4 of observed STD. The simulated SST had underestimated spatial variability in April and overestimated

variability in July (Figure 4d) and August (Figure 4e) – the ratio between STD was either less than or larger than 1 for all different days in the corresponding month, respectively. In other months, the ratio between observed and simulated STD varied from 0.55 to 1.3. The RMSD for all the months was less than 1.2 of observed STD. The lowest correlation between GETM and MODIS data within one day was 0.4 (July 2015) and the highest 0.93 (July 2012), while the median value for correlation was 0.85.

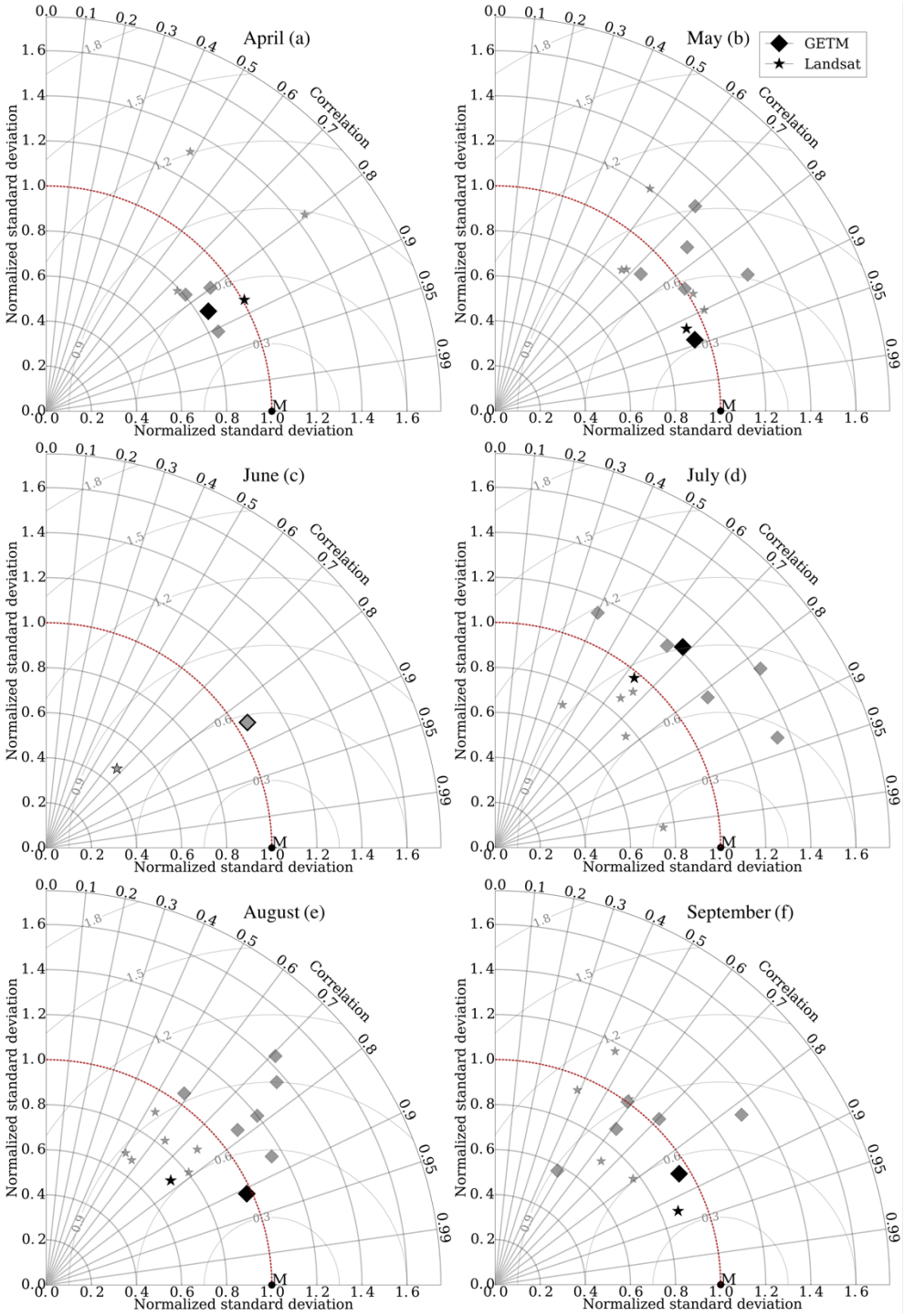

Figure 4. Taylor diagrams for different months. Black markers indicate to each month composite results from period 2012–2015. Grey markers are results from all different days in a corresponding month. The reference point M denotes to MODIS. The most concurring points with MODIS are the closest to reference points. More close markers to red line has the most similar STD with MODIS.

3.2 Qualitative data comparison

Examples of GETM, MODIS and Landsat SST fields for selected dates with large spatial coverage are shown in Figure 5. Landsat SST field was retrieved from brightness temperature by using the correction algorithm based on previously described statistical differences between Landsat and MODIS data (see section 3.1). The algorithm worked relatively well – the large-scale patterns of high-resolution SST fields looked very similar with MODIS observations and only in some cases a larger bias between Landsat and MODIS remained.

The simulated SST was underestimated for the open parts of the sea during the seasonal heating period (April–May) and overestimated during the summer (August). In coastal areas, the simulated SST was slightly overestimated as for example in 4th of August when narrow high temperature front was observed along the Latvian coast in Baltic Proper expanding up to the north until the southern entrance of the Gulf of Finland. In addition, the overestimated temperatures were also observed in the eastern parts of the Gulf of Riga and semi-enclosed Väinameri, located between Gulf of Finland and Gulf of Riga. Despite the differences in SST values, similar eddy activity was observed in the northern part of the Gulf of Finland on 4th of August. Cold water upwelling front along the northern part of the Gulf of Finland caused by the wind forcing (well documented by Haapala 1994; Uiboupin and Laanemets 2009) in the region with long filaments extending to the central part of the Gulf, was visible in all SST products (see Figure 5). The extent of the upwelling area was slightly overestimated with the simulation, which was most likely due to the model resolution. Väli et al (2016) showed that the simulated upwelling area in the Gulf of Finland depends also on the horizontal resolution used in simulations. Similar dependence of upwelled water temperature on the horizontal resolution of the model was shown by Vankevich et al. (2016). Temperatures measured by the Landsat in the upwelling front were slightly overestimated, but the extent of upwelling front was comparable with MODIS measurements.

The SST products for the 20th of August indicated an upwelling along the southern coast of the Gulf of Finland. The extent of the upwelling area was the largest in MODIS observations, while the simulated temperatures were overestimated both in the coastal and open sea areas of the different basins. In the middle of the upwelling front, the simulated SST values were comparable with the MODIS observations, indicating vertical transport from the same depth levels.

The impact of diurnal cycle of heating and cooling was also visible. The time lag for some of the images was more than 8 hours. Uiboupin and Laanemets (2014) have showed that wind speed significantly influenced the bias between *in situ* and satellite data, which means that the time difference more than 8 hours and wind conditions could also impact bias between Landsat and MODIS data.

In general, spatial variability of Landsat and MODIS SST fields was similar with clearly visible mesoscale structures in both datasets and submesoscale structures in Landsat data. The simulated SST patterns (eddies and fronts) on GETM fields were more pronounced, but the extent was most likely overestimated.

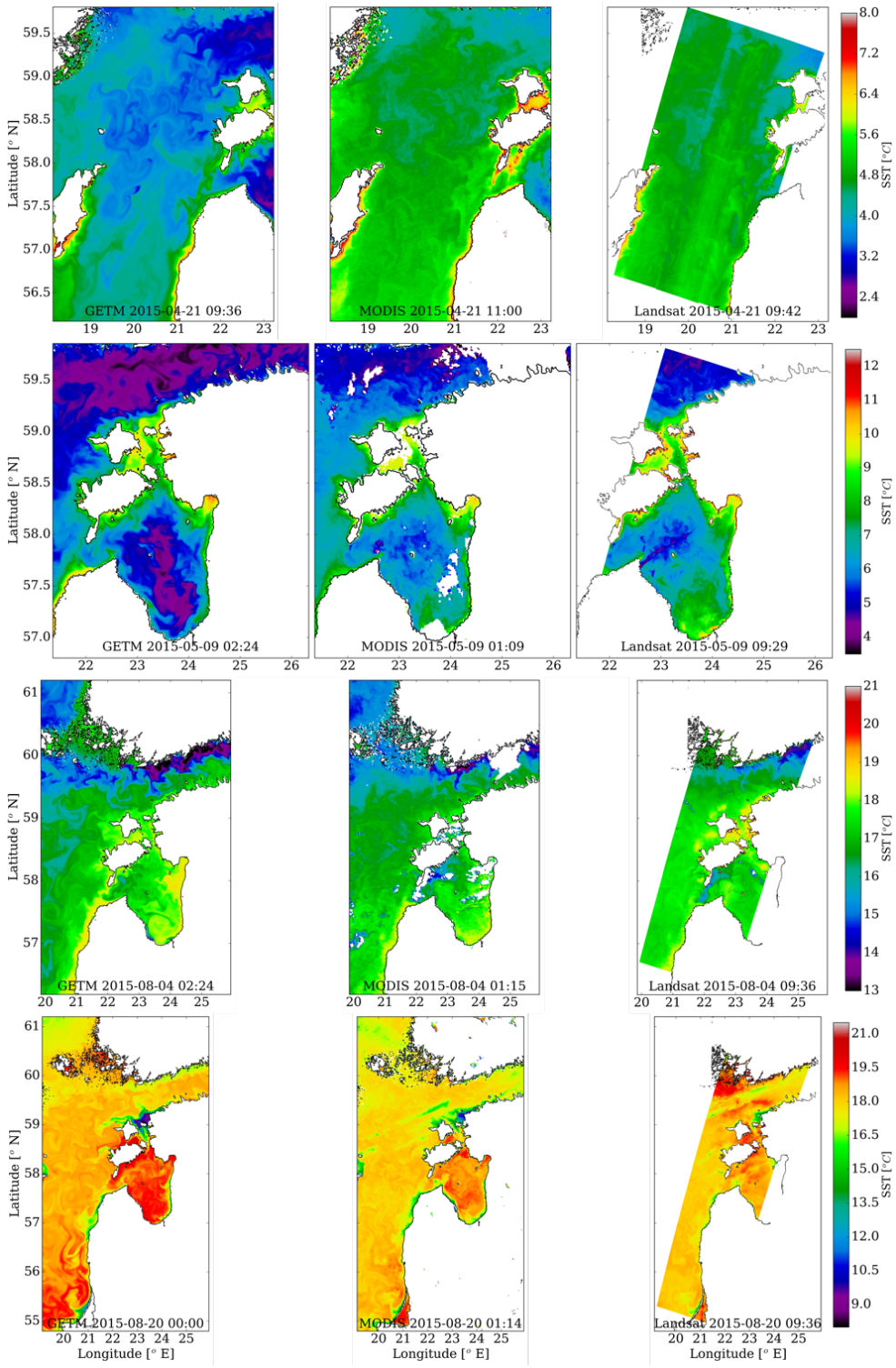

Figure 5. Comparison of GETM, MODIS and Landsat surface temperature distributions. Landsat temperature data were corrected with MODIS temperature data. All three datasets are on their original grid.

3.3 Submesoscale features

3.3.1 Gradient analysis of submesoscale structures

For investigating submesoscale processes, spatial resolution is an important factor. Figure 6 shows the impact of horizontal resolution in studying (sub)mesoscale structures. Spatial resolution of Landsat SST fields is approximately 30 m, while MODIS has only 1000 m resolution. Although the filament of upwelled water with lower temperature compared to surrounding water temperature was visible on both products (Figure 6a), the Landsat produced much more detailed image of the SST field (Figure 6b). The SST on the Landsat image was overestimated even after the application of statistical correction algorithm, but patterns on Figure 6a and Figure 6b match very well. The cyclonic filament has not yet formed into a cyclonic eddy, warmer temperatures are seen in the south from the top of filament extending to the west from the centre of the filament and lower temperatures associated with the upwelling front are seen in the north-west on both datasets.

Väli et al. (2016) showed that simulation with grid size of 0.125 nautical miles (~230 m) revealed different forms of submesoscale structures in the Gulf of Finland, while lower resolution simulations were not able to resolve those features.

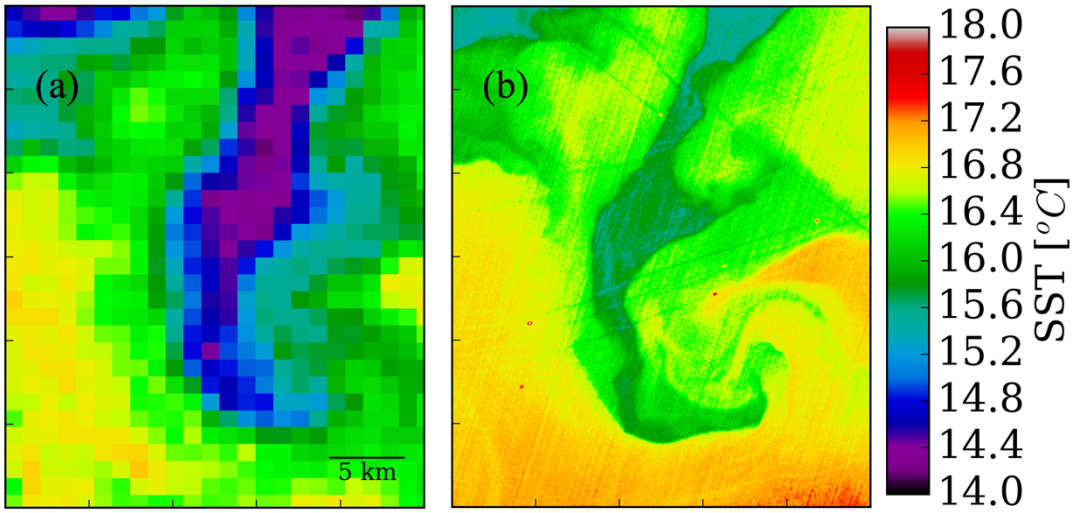

Figure 6. Same upwelling filament on MODIS (a) and Landsat (b) image. Eddy locations are shown on Figure 1 for 2015–08–04 image with a) and b).

An example of upwelling along the southern coast of Gulf of Finland with SST gradients from the area and the distribution of gradient magnitudes from different datasets are shown in Figure 7. The upwelling patterns were similar in all different SST products, but the temperature values differed slightly. Landsat SST (Figure 7c) overestimated temperature values approximately 2 ^{o}C in the centre of the upwelling area, however, same eddies were seen on both observations (MODIS image, Figure 7b and Landsat, Figure 7c). The simulated upwelling area and intensity were slightly overestimated (Figure 7a). The temperature of upwelled water was lower compared to the MODIS data, while the open sea temperature was slightly higher. Hence the upwelling front in the simulation was also sharper compared with the observations. Interestingly sharper front can be seen also on the Landsat product, which has high temperature comparable with simulated SST in the open parts of the sea, but near the coast temperature was also overestimated.

The SST gradient magnitudes were the largest in the Landsat images (Figure 7d–f). The largest values exceeded 3 ^{o}C/km in very small areas (elongated thin stripes separating different water masses) and were visible only on high resolution SST fields as the gradient magnitudes calculated from MODIS and simulation data were

less than 1.5 ^{o}C /km. The distributions of GETM SST gradients were similar for different dates (Figure 7g, j and m) with gradient peak values close to 0.05 ^{o}C/km and distributions relatively symmetric. MODIS gradient peaks were close to 0.1 ^{o}C/km and distributions similarly with simulated gradients relatively symmetric. Nevertheless, the kurtosis is much larger and scale parameter smaller for MODIS distributions compared to the GETM (Figure 7h, k). In the same time Landsat revealed the asymmetry of the distributions. In addition, the minimum gradients in the Landsat were larger compared to the MODIS and GETM and the peak values were close to 1 ^{o}C/km for different dates (Figure 7i, l, n).

In general, the weakest gradients were in the simulated SST and the strongest gradients in the high resolution SST fields. Most likely the simulated SST gradient was underestimated due to strong lateral mixing in the surface layers and too coarse resolution compared to the Landsat observations.

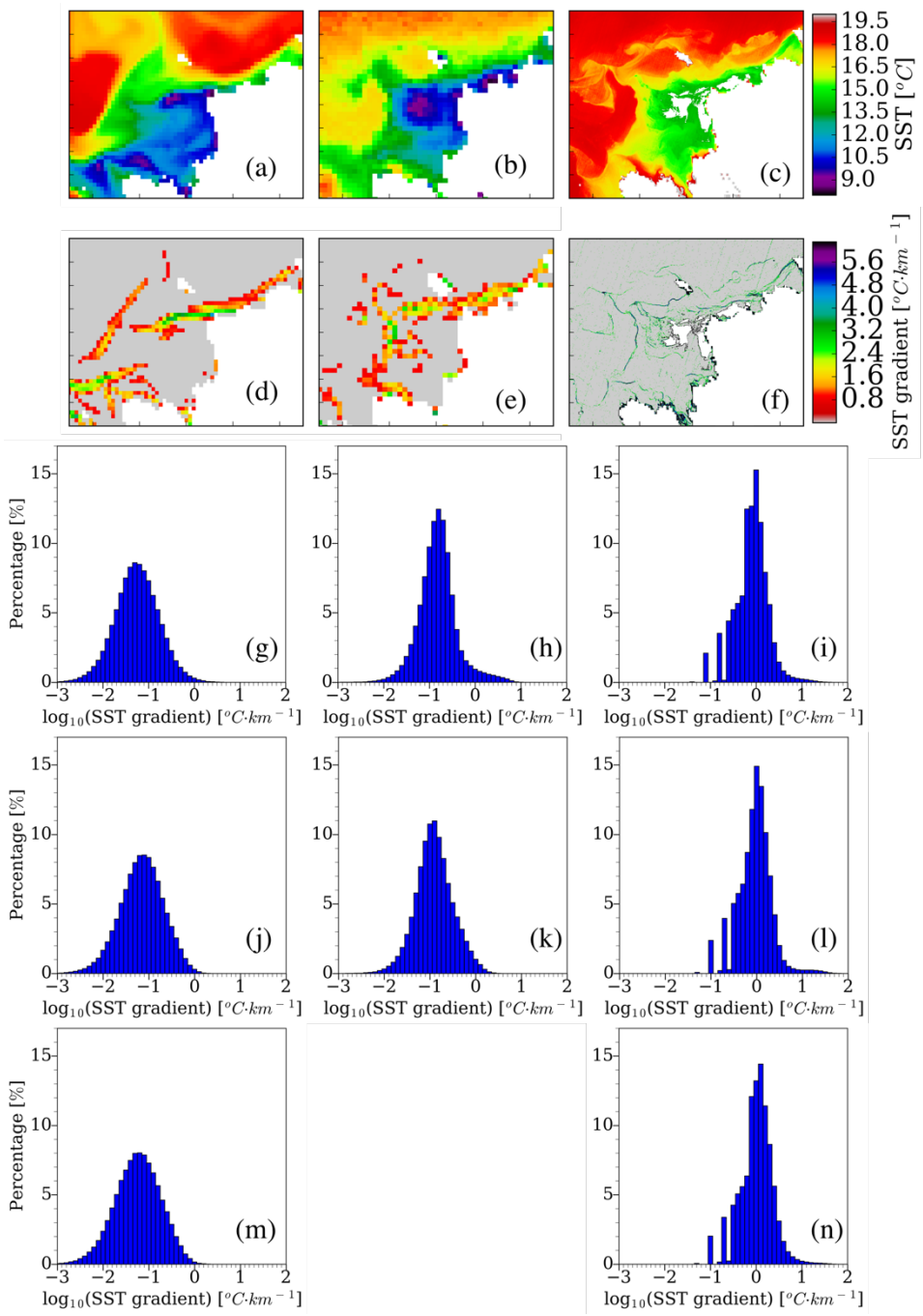

Figure 7. SST, SST gradient and gradient histograms from West Coast of Estonia for GETM (left), MODIS (middle) and Landsat (right). SST field for August 20, 2015 is shown on panels a–i Histograms only are shown for May 9, 2015 (panels j–l) and May 3, 2013 (panels m–n).

Vazquez-Cuervo et al. (2013) also showed that the higher resolution data provided more realistic representation of the location and magnitudes of the SST fronts off coast Peru. However, they performed measurements in the Pacific Ocean, where sub- and mesoscale features tend to be with larger scale than in the Baltic Sea due to larger baroclinic Rossby radius of deformation. Same authors also found that migration of gradients observed in the multi-scale ultra-high resolution sea surface temperature fields with 1 km resolution captured mesoscale to submesoscale features. In that study the SST gradients from other three datasets with lower resolution (Operational Sea Surface Temperature and Sea Ice Analysis, Remote Sensing Systems microwave infrared merged SST analysis, A Group for High Resolution Sea Surface Temperature) did not reveal submesoscale features. In current study, it was also found that the dataset with higher resolution (Landsat) captured features in range from mesoscale to submesoscale, while other two (MODIS and GETM) did not resolve submesoscale features.

3.3.2 Spectral analysis of submesoscale structures (sensors)

The mean PSD in wavenumber space calculated from MODIS, Landsat and GETM SST datasets for different regions are shown in Figure 8. In the low frequency range (4−10 km for GETM and MODIS) the spectral slopes of GETM SST were the steepest (Figure 8 a–c) with slope values from −5.55 to −3.87 in the log-log space (the mean value is −4.89 see Table 3). The shallowest spectral slope in the low frequency range was for the MODIS SST with mean value of −2.52, while the spectral slope in the low frequency range for Landsat SST (2−10 km) varied from −4.89 to −3.07 (mean slope was −3.95). As the horizontal resolution of the Landsat SST product is 30 m, the PSD was calculated in the high frequency range (0.15−2 km). The mean spectral slope in the high frequency range was −1.91. The spectral slope −2 is important as it characterizes the proper energy transfer from smaller wavelengths to the larger wavelengths and hence the existence of submesoscale features in the dataset. In the current analysis the SST subsets with spectral slopes

close to −2 were for example subset (k) with spectral slope −1.88 and subset (h) with spectral slope −1.96 (Table 3). However, there were subsets, which did not show the presence of submesoscale features in high resolution Landsat SST field: for example subset (o), where spectral slope was −3.15 (Table 3) and was also depicted in Figure 8.

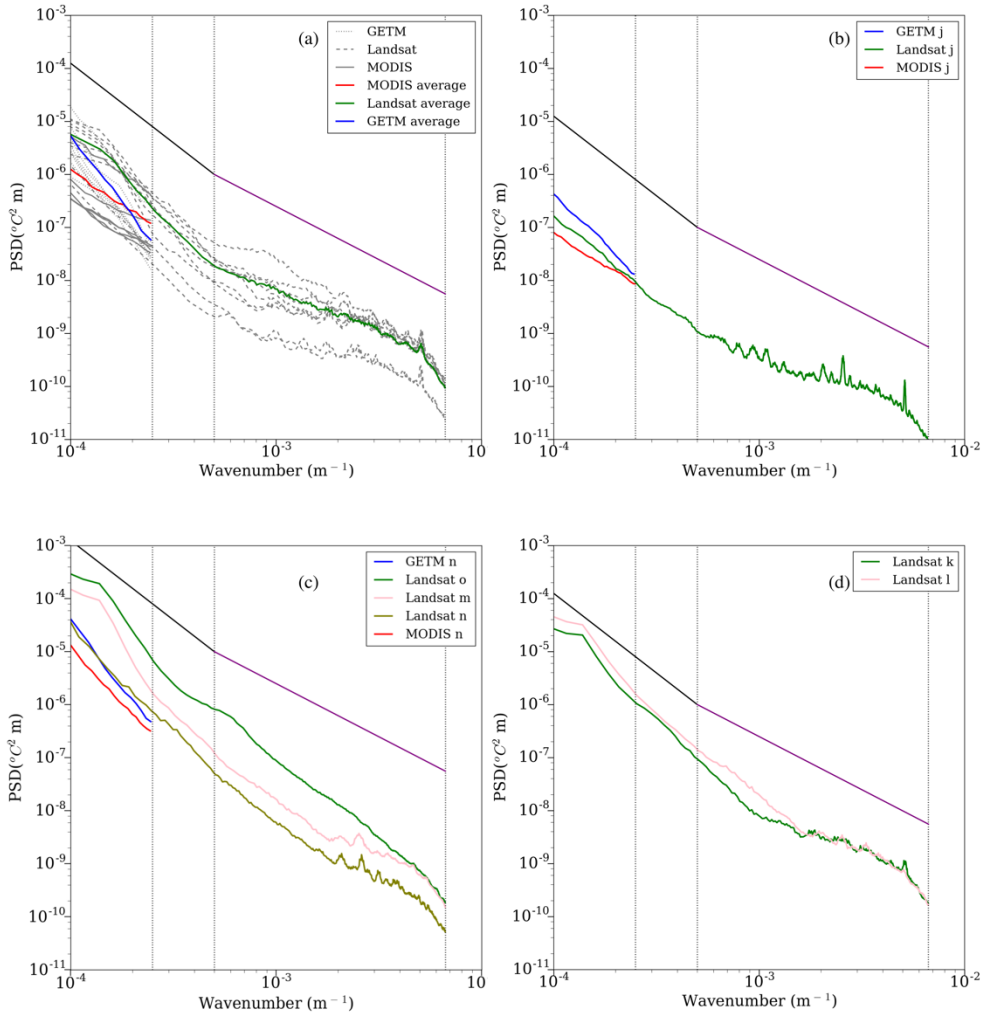

Figure 8. Mean wavenumber spectra for SST in the Baltic Proper (BP) (a), Gulf of Finland (GOF) (c) and Gulf of Riga (GOR) (d). Letters in the legend refer to the different subsets used to calculate the spectra. On panel a) the grey lines represent different days, coloured lines the averaged spectra over BP area. Vertical dotted lines are wavenumbers corresponding to 4 km (left), 2 km (middle) and 0.15 km (right). Spectral slopes –3 (black) and –2 (purple) in log-log space are shown on all panels.

3.3.3 Spectral analysis of meso- and submesoscale structures in different regions

Similar SST patterns were observed from MODIS, Landsat and GETM products in three basins of the Baltic Sea – Gulf of Riga, Gulf of Finland and Baltic Proper. In order to analyse the submesoscale activity in different regions the spectral slopes from Landsat SST fields in all three regions were compared. As the Gulf of Riga and Gulf of Finland have small baroclinic Rossby radius, the submesoscale features were poorly resolved in MODIS and GETM data. Väli et al (2016) showed that simulation with 0.125 nautical mile resolution resolve the submesoscale structures in the Gulf of Finland.

The spectral slope in low frequency range for the Baltic Proper in Landsat SST fields varied from −4.85 to −3.07, while the slope in the Gulf of Riga varied from −4.01 to −3.84 and in the Gulf of Finland from −4.89 to −3.75. Slope −4.85 was determined from subset (d) (see Figure 1) and there were several eddies observed. In the same time, slope −3.07 was determined from the larger area, subset (j) (Figure 1) and there were more mesoscale structures present.

The PSD calculated from Landsat SST fields displayed clear difference between high frequency and low frequency range, the spectral slope was much shallower in high frequency compared to the low frequency range. In the Gulf of Finland the spectral slope varied from −3.15 to −2.13 and in the Gulf of Riga from −2.21 to −1.88. In the Baltic Proper the spectral slopes in high frequency range were even smaller (from −2.37 to −1.45), however −2.37 was exceptional in that area, which could be explained with minimal temperature fluctuation on subset (g).

In most of the studied cases submesoscale features occurred on Landsat SST field. However, on subset (o) the spectral slope was steeper than −3, i.e. there were no submesoscale structures present on the SST image for that day (Table 3). The SST field in subset (o) was very homogenous and eddies or other forms of submesoscale structures (threads, fronts) were not observed.

Table 3. GETM, MODIS and Landsat mean wavenumber spectra slopes in log-log space from subsets a to o, which locations are shown on Figure 1. Averaged slope values are on the last row.

Subset	Date	Area	GETM (4–10 km)	MODIS (4–10 km)	Landsat (2–10 km)	Landsat (0.15–2 km)
a	2015–04–21	BP	–4.05	–2.51	–3.73	–1.66
b	2015–04–21	BP	–4.93	–2.29	–4.65	–1.45
c	2015–04–21	BP	–5.07	—	–3.73	–1.56
d	2015–04–21	BP	–4.41	–2.12	–4.85	–1.47
e	2015–08–04	BP	–5.49	—	–3.69	–1.78
f	2015–08–04	BP	–5.50	—	–3.40	–1.79
g	2015–08–04	BP	–5.04	–1.77	–3.79	–2.37
h	2015–08–04	BP	–4.98	–2.74	–3.94	–1.96
i	2015–04–21	BP	–5.55	–2.37	–3.62	–1.46
j	2015–04–21	BP	–3.87	–2.34	–3.07	–1.56
k	2015–05–09	GOR	—	—	–3.84	–1.88
l	2015–05–09	GOR	—	—	–4.01	–2.21
m	2015–05–09	GOF	—	—	–4.89	–2.13
n	2015–08–04	GOF	–4.92	–4.05	–3.75	–2.28
o	2013–05–03	GOF	—	—	–4.30	–3.15
Mean			–4.89	–2.52	–3.95	–1.91

Charney (1971) showed that according to quasi-geostrophic theory PSD should follow the slope −3 (in the log-log space) in the inertial range when applied to mesoscale eddies. In this study, mean PSD slope varied from −4.89 to −2.52. Capet et al (2008a, 2008b) showed that submesoscale structures caused shallower spectral slope, close to value −2. Several studies (e.g. Brannigan et al. 2015; Lips et al. 2016;

Väli et al. 2016) also showed that the presence of submesoscale processes caused shallower spectral slope. In current study the mean spectral slope of high resolution SST data in high frequency range was −1.91, which is close to −2.

Lips et al. (2016) using the multi-sensor high resolution in situ observations in the Gulf of Finland found that when there are pronounced mesoscale features, PSD slope is shallower than −2. They also showed that, when the spatial variability was caused by the coastal upwelling events, wavenumber spectra of density variance was close to −2 slope (Lips et al. 2016). Current study confirms also that in the Gulf of Finland in cases of active mesoscale processes the spectral slope of two-dimensional SST field was close to −2, except subset (o) where mesoscale activity was low (STD was as small as 0.17 ^{o}C) and submesoscale processes were not present.

4 CONCLUSIONS

Comparing quantitatively GETM and Landsat SST data with MODIS SST data differences between the datasets were estimated. Systematic bias between MODIS and Landsat SST was found. An empirical algorithm was constructed to correct the Landsat brightness temperature and retrieve high resolution SST fields for the period 2012–2015.

The correlation between monthly MODIS and Landsat and MODIS and GETM SST was high and varied from 0.63 to 0.94. The root mean square difference (RMSD) varied within a range from 0.41 to 0.95 °C. The largest differences were on August. The RMSD between MODIS and GETM was from 0.82 to 1.23 °C. The structures from Landsat and MODIS SST quantitatively match slightly better than the GETM and MODIS SST. Nevertheless, the daily means were highly correlated (R=0.99) with the MODIS observations for both the Landsat and GETM SST. Taylor diagrams indicated that MODIS and GETM data were more similar compared to the Landsat.

Qualitative data comparison confirmed that correction algorithm for high resolution Landsat SST data worked well. In some cases, the Landsat SST was overestimated. The Landsat and MODIS SST fields have similar variability with collocated mesoscale structures in both datasets. The GETM SST patterns were more pronounced, but the structures did not collocate with the corresponding structures on satellite SST products.

The gradient analysis indicated that the Landsat (resolution 30 m) SST gradient magnitudes were more detailed compared to the MODIS (resolution 1000 m) and

GETM (resolution 926 m) SST gradients. Landsat SST gradients varied more with most of the values around 1 ^{o}C/km. The GETM gradients for the same time moments had most of the values around 0.05 ^{o}C/km and MODIS around 0.1 ^{o}C/km.

Mean wavenumber spectra showed that in the low frequency range (4–10 km) the spectral slope in the log-log space was the steepest for GETM SST fields (mean slope −4.89), while the MODIS had the shallowest spectral slope (mean slope −2.52). The mean spectral slope for Landsat SST in the low frequency range (2-10 km) was −3.95. In the high frequency range (0.15–2 km), only the Landsat data was available and the mean slope was −1.91, which was very close to the theoretical spectral slope for submesoscale features (−2).

Similar patterns in MODIS, Landsat and GETM SST fields were seen in Baltic Proper, Gulf of Finland and Gulf of Riga. The regional differences were best captured by the Landsat SST fields and spectral analysis indicated a spectral slope from −4.85 to −3.07 for SST in Baltic Proper, −4.89 to −3.75 for Gulf of Finland and −4.01 to −3.84 for Gulf of Riga in low frequency range.

In high frequency range, the spectral slopes varied from −2.37 to −1.45 in the Baltic Proper, from −2.21 to −1.88 in the Gulf of Riga and from −3.15 to −2.13 in the Gulf of Finland. Nevertheless, in some of the subsets of Landsat SST spectral slopes did not indicate the presence of submesoscale features. In these cases the mesoscale activity were low and SST fields were very homogeneous.

REFERNCES

Alenius, P., Nekrasov, A. and Myrberg, K. 2003. Variability of the baroclinic Rossby radius in the Gulf of Finland. *Continental Shelf Research,* 23(6), 563–573.

Alpers, W., Brandt, P., Lazar, A., Dagorne, D., Sow, B., Faye, S., Hansen, W. M., Rubino, A., Poulain, P-M. and Brehmer, P. 2012. A small-scale oceanic eddy off the coast of West Africa studied by multi-sensor satellite and surface drifter data. *Remote Sensing of Environment,* 129, 132–143.

Andrejev, O., Sokolov, A., Soomere, T., Värv, R. and Viikmäe, B. 2010. The use of high- resolution bathymetry for circulation modelling in the Gulf of Finland. *Estonian Journal of Engineering,* 16(3), 187–210.

Andrejev, O., Soomere, T., Sokolov, A. and Myrberg, K. 2011. The role of the spatial resolution of a three-dimensional hydrodynamic model for marine transport risk assessment. *Oceanologia,* 53(1), 309–334.

Baltic Sea Hydrographic Commission. 2013. *Baltic Sea Bathymetry Database version 0.9.3*. (Online). http://data.bshc.pro/ (06.07.2016)

Bouffard, J., Renault, L., Ruiz, S., Pascual, A., Dufau, C. and Tintoré, J. 2012. Sub-surface small-scale eddy dynamics from multi-sensor observations and modeling. *Progress in Oceanography* 106, 62–79.

Brannigan, L., Marshall, P D., Naveira-Garabato, A. and Nurser, A. J. G. 2015. The seasonal cycle of submesoscale flows. *Ocean Modelling,* 92, 69–84.

Brown, O. B. and Minnett, P. J. 1999. MODIS infrared sea surface temperature algorithm theoretical basis document, ver.2.0. (Online). http://modis.gsfc.nasa.gov/data/atbd/atbd_mod25.pdf (16.02.2017)

Buckingham, E. C., Garabata, C. N. A., Thompson, F. A., Brannigan, L., Lazar, A., Marshall, P. D., Nurser, A. J. G., Damerell, G., Heywood, J. K. and Belcher, E. S. 2016. Seasonality of submesoscale flows in the oceansurface boundary layer. *Geophysical Research Letters,* 43(5), 2118–2126.

Burchard, H. and Bolding, K. 2001. Comparative analysis of four second-moment turbulence closure models for the oceanic mixed layer. *Journal of Physical Oceanography*, 31, 1943–1968.

Burchard H., Bolding, K. and Villarreal, M.R. 2004. Three-dimensional modelling of estuarine turbidity maxima in a tidal estuary. *Ocean Dynamics*, 54: 250–265.

Canuto, V. M., Howard, A., Cheng, Y. and Dubovikov M. S. 2001. Ocean Turbulence. Part I: One-Point Closure Model—Momentum and Heat Vertical Diffusivities. *Journal of Physical Oceanography.* http://dx.doi.org/10.1175/1520-0485(2001)031<1413:OTPIOP>2.0.CO;2

Capet, X., McWilliams, J.C., Olemaker, M. J. M. and Shchepetkin, A. F. 2008a. Mesoscale to Submesoscale Transition in the California Current System. Part I: Flow structure, Eddy Flux, and Observational Tests. *Journal of Physical Oceanography,* 38(1), 29–43.

Capet, X., McWilliams, J.C., Olemaker, M.J.M. and Shchepetkin, A. F. 2008b. Mesoscale to Submesoscale Transition in the California Current System. Part III: Energy Balance and Flux. *Journal of Physical Oceanography,* 38(10), 2256–2269.

Charney, J. G. 1971. Geostrophic Turbulence. *Journal of the Atmospheric Sciences,* 28(6), 1087–1095.

Feldman, C. G. 2016. Ocean ColorWeb. (Online).
https://oceancolor.gsfc.nasa.gov/cgi/browse.pl (10.09.2015)

Fennel, W., Seifert, T. and Kayser B. 1991. Rossby radii and phase speeds in the Baltic Sea. *Continental Shelf Research,* 11(1), 23–36.

Ferrari, R. and Wunsch, K. 2009. Ocean Circulation Kinetic Energy: Reservoirs, Sources, and Sinks. *Annual Review of Fluid Mechanics,* 41, 253–282.

Gräwe, U., Holtermann, P., Klingbeil, K. and Burchard, H. 2015. Advantages of vertically adaptive coordinates in numerical models of stratified shelf seas. *Ocean Modelling,* 92, 56–68.

Gurova, E. and Chubarenko, B. 2012. Remote-sensing observations of coastal sub-mesoscale eddies in the south-eastern Baltic. *Oceanologia,* 54(4), 631–654.

Haapala, J. 1994. Upwelling and its Influence on Nutrient Concentration in the Coastal Area of the Hanko Peninsula, Entrance of the Gulf of Finland. *Estuarine, Coastal and Shelf Science,* 38(5), 507–521.

Hofmeister, R., Burchard, H. and Beckers, J-M. 2010. Non-uniform adaptive vertical grids for 3D numerical ocean models. *Ocean Modelling,* 33(1–2), 70–86.

Kahru M., Hakansson B. and Rud, O. 1995. Distributions of the sea-surface temperature fronts in the Baltic Sea as derived from satellite imagery. *Continental Shelf Research,* 15(6), 663–679.

Karimova, S. S., Lavrova Yu. O. and Solovev, M. 2012. Observation of Eddy Structures in the Baltic Sea with the Use of Radiolocation and Radiometric Satellite Data. *Atmospheric and Oceanic Physics,* 48(9), 1006–1013.

Karimova, S. and Gade, M. 2016. Improved statistics of sub-mesoscale eddies in the Baltic Sea retrieved from SAR imagery. *International Journal of Remote Sensing,* 37(10), 2394–2414.

Kikas, V. and Lips, U. 2016. Upwelling characteristics in the Gulf of Finland (Baltic Sea) as revealed by Ferrybox measurements in 2007-2013. *Ocean Science*, 12, 843−859.

Laanemets, J., Väli, G., Zhurbas, V., Elken, J., Lips, I. and Lips, U. 2011. Simulation of mesoscale structures and nutrient transport during summer upwelling events in the Gulf of Finland in 2006. *Boreal Environment Research,* 16, 15–26.

Lehmann, A., Myrberg, K. and Höflich, K. 2012. A statistical approach to coastal upwelling in the Baltic Sea based on the analysis of satellite data for 1990–2009. *Oceanologia*, 54(3), 369–393.

Leppäranta, M. and Myrberg, K. 2009. *Physical Oceanography of the Baltic Sea*. Chichester: Springer.

Lips, U. and Lips, I. 2014. Bimodal distribution patterns of motile phytoplankton in relation to physical processes and stratification (Gulf of Finland, Baltic Sea). *Deep Sea Research Part II: Topical Studies in Oceanography,* 101, 107–119.

Lips, U., Zhurbas, V., Skudra, M. and Väli, G. 2016. A numerical study of circulation in the Gulf of Riga, Baltic Sea. Part II: Mesoscale features and freshwater transport pathways. *Continental Shelf Research,* 115, 44–52.

Liu, F., Tang, S. and Chen, C. 2015. Satellite observations of the small-scale cyclonic eddies in the western South China Sea. *Biogeosciences,* 12, 299–305.

Maljutenko, I. and Raudsepp, U. 2014. Validation of GETM model simulated long-term salinity fields in the pathway of saltwater transport in response to the Major Baltic Inflows in the Baltic Sea. 2014 IEEE/OES Baltic International Symposium

(BALTIC 2014): 2014 IEEE/OES Baltic International Symposium, Tallinn, 24–27.04.2014. Institute of Electrical and Electronics Engineers (IEEE), 23−31.

Matthäus, W. and H. Franck. 1992. Characteristics of major Baltic inflows—A statistical analysis. *Continental Shelf Research*, 12, 1375–1400.

Mälkki, P. and Tamsalu, R. 1985. Physical features of the Baltic Sea. *Finnish Marine Research,* 252, 110. http://hdl.handle.net/10138/167788

Männik, A. and Merilain, M. 2007. Verification of different precipitation forecasts during extended winter-season in Estonia. *HIRLAM Newsletter*, 52, 65–70.

OceanColor Web. 2015. (Online). https://oceancolor.gsfc.nasa.gov/cgi/browse.pl (10.10.2015)

Ohlmann, J. C., Molemaker, M. J., Baschek, B., Holt, B., Marmorino, G. and Smith, G. 2017. Drifter observations of submesoscale flow kinematics in the coastal ocean. *Geophysical Research Letters,* 44(1), 330–337.

Oreopoulos, L., Wilson, J. M. and Varnai, T. 2011. Implementation on Landsat Data of a Simple Cloud-Mask Algorithm Developed for MODIS Land Bands. *IEEE Geoscience and Remote Sensing Letters,* 8(4), 597–601.

Robinson, R. A. 1983. *Eddies in Marine Science.* Berlin: Springer-Verlag Berlin Heidelberg.

Reinart, A. and Reinhold, M. 2008. Mapping surface temperature in large lakes with MODIS data. *Remote Sensing of Environment*, 112(2), 603–611.

Reißmann, J.H. 2005. An algorithm to detect isolated anomalies in three-dimensional stratified data fields with an application to density fields from four deep basins of the Baltic Sea. *Journal of Geophysical Research,* 110(C12), 1–17.

Reißmann, J.H. 2006. On the representation of regional characteristics by hydrographic measurements at central stations in four deep basins of the Baltic Sea. *Ocean Science,* 2, 71–83.

Soomere, T., Myrberg, K. and Leppäranta, M. 2008. The progress in knowledge of physical oceanography of the Gulf of Finland: a review for 1997–2007*. *Oceanologia,* 50(3), 287–362.

Stips, A., Bolding, K., Burchard, H., Djavidnia, S. and Peneva, E. 2005. Realistic multiannual simulations of the coupled North Sea and Baltic Sea system using the GETM model. Italy: European Communities.

Thomas, L. N., Tandon, A. and Mahadevan, A. 2008. Submesoscale processes and dynamics. *Journal of Geophysical Research,* https://doi.org/10.1029/177GM04

Uiboupin, R. and Laanemets, J. 2009. Upwelling characteristics derived from satellite sea surface temperature data in the Gulf of Finland, Baltic Sea. *Boreal Environment Research,* 14(2), 297–304.

Uiboupin, R. and Laanemets, J. 2014. Upwelling Parameters from Bias-Corrected Composite Satellite SST Maps in the Gulf of Finland (Baltic Sea). *IEEE Geoscience and Remote Sensing Letters,* 12(3), 592–596.

Umlauf, L. and Burchard, H. 2005. Second-order turbulence closure models for geophysical boundary layers. A review of recent work. *Continental Shelf Research,* 25(7–8), 795–827.

USGS. 2016. Using the USGS Landsat 8 Product. (Online).
https://landsat.usgs.gov/using-usgs-landsat-8-product (11.10.2015)

Vahtera, E., Laanemets, J., Pavelson, J., Huttonen, M. and Kononen, K. 2005. Effect of upwelling on the pelagic environment and bloom-forming cyanobacteria in the western Gulf of Finland, Baltic Sea. *Journal of Marine Systems*, 58, 67–82.

Vankevich, E. R., Sofina V. E., Eremina, E. T., Ryabchenko, A. V., Molchanov, S. M. and Isaev, V. A. 2016. Effects of lateral processes on the seasonal water stratification of the Gulf of Finland: 3-D NEMO-based model study. *Ocean Science,* 12(4), 987–1001.

Vazquez-Cuervo, J., Dewitte, B., Chin, M. T., Armstrong, M. E., Purca, S. and Alburquequed, E. 2013. An analysis of SST gradients off the Peruvian Coast: The impact of going to higher resolution. *Remote Sensing of Environment,* 131, 76–84.

Väli, G., Zhurbas, G., Lips, U. and Laanemets, U. 2016. Submesoscale structures related to upwelling events in the Gulf of Finland, Baltic Sea (numerical experiments). *Journal of Marine Systems*. http://dx.doi.org/10.1016/j.jmarsys.2016.06.010

Quentel, E., Carton, X., Gutscher, M.-A. and Hobbs, R. 2010. Detecting and characterizing mesoscale and submesoscale structures of Mediterranean water from joint seismic and hydrographic measurements in the Gulf of Cadiz. *Geophysical Research Letters,* 37(6), 1–5.

Acknowledgements

Author thanks Rivo Uiboupin and Germo Väli for their guidance and valuable comments. Author is grateful to Sander Rikka for applying Fast Fourier Transform to subsets used in this study.

RESÜMEE

Leidmaks andmetevahelised erinevused, võrreldi MODIS'e andmeid Landsat'i ja GETM'i andmetega kvantitatiivselt. Landsat'i ja MODIS'e andmete vahel leiti süstemaatiline viga. Seetõttu koostati empiiriline algoritm MODIS'e ja Landsat'i andmete vahel kasutades perioodi 2012–2015 andmeid. Algoritmi abil koostati Landsat'i heledustemperatuurist kõrglahutuslikud pinnavee temperatuuri väljad.

MODIS'e ja Landsat'i ühe kuu andmete vaheline korrelatsioon varieerus 0.63-st 0.93-ni ja GETM'i ning MODIS'e vahel 0.63-st 0.94-ni. Ruutkeskmine erinevus varieerus vahemikus 0.41 kuni 0.95 ^{o}C. Erinevused olid kõige suuremad augustis. Statistilised parameetrid näitavad, et Landsat'i ja MODIS'e struktuurid kattuvad natukene paremini kui GETM'il ja MODIS'el, aga päevased keskmised korreleeruvad mõlemate andmetega väga hästi (R=0.99).

Kvalitatiivne võrdlus kinnitab, et algoritm kõrgelahutusega pinnavee temperatuuri andmete saamiseks Landsat'i heledustemperatuurist töötas hästi, kuigi mõningatel juhtudel Landsat jätkuvalt ülehindab temperatuuri väärtuseid. Landsat'i ja MODIS'e pinnavee temperatuuri väljades on näha sarnast muutlikust ning sub- ja mesomastaapsete keeriste struktuurid asuvad samades kohtades. GETM'i pinnavee temperatuuri simulatsioonides on keerised näha, kuid tihti ei kattu nende asukoht satelliidipiltidelt tuvastatud keeristega.

Gradientanalüüs näitas, et Landsat'i (resolutsioon 30 m) pinnavee temperatuuri absoluutsed gradiendid olid detailsemad, kui MODIS'e (resolutsioon 1000 m) ja GETM'i (resolutsioon 926 m) gradiendid. Landsat'i absoluutsed gradiendi väärtused

varieerusid kõige rohkem ning suurim hulk väärtuseid oli 1 ^{o}C/km ümber. Samal ajal MODIS'e temperatuuri gradiendi väärtuste tipp jäi 0.1 ^{o}C/km juurde ning GETM'i temperatuuri gradiendi tipp oli 0.05 ^{o}C/km ümber.

Spektraalanalüüs näitas, et 4–10 km vahemikus on spektrikalle kõige järsem GETM'i pinnavee temperatuuri väljades (–4.89) ning kõige laugem MODIS'e andmetes (–2.52). Keskmine spektrikalle Landsat'i andmetes oli –3.95. Vahemik 0.15–2 km kirjeldab submesomastaapseid nähtuseid ning seda kirjeldavad ainult Landsat'i andmed. Antud vahemikus oli keskmine spektrikalle –1.91, mis on lähedal teoreetilisele kaldele, mis kirjeldavad submesomastaapseid nähtuseid (–2).

MODIS'e, Landsat'i ja GETM'i pinnavee temperatuuri väljadest oli näha sarnaseid jooni Läänemere avaosas, Liivi lahes ja Soome lahes. Asukohapõhised erinevused olid kõige paremini märgatavad Landsat'i andmetest. Spektraalanalüüs mesomastaapses vahemikus (2-10 km) näitas, et Läänemere avaosas varieerub kalle −4.85 kuni −3.07, Soome lahes −4.89 kuni −3.75 ja Liivi lahes −4.01 kuni −3.84.

Vahemikus 0.15–2 km jäid spektraalkalded Läänemere avaosas vahemikku –2.37 kuni –1.45, Liivi lahes –2.21 kuni –1.88 ja Soome lahes –3.15 kuni –2.13. Mõnel juhul Landsat'i andmetest submesomastaapseid nähtuseid ei tuvastatud ning neil juhtudel olid ka pinnavee temperatuuri väljad homogeensed.